Electronic Supplementary Material to: Factors Influencing the Spatial Variability of Air Temperature Urban Heat Island Intensity in Chinese Cities*

Heng LYU[1], Wei WANG[1,2], Keer ZHANG[3], Chang CAO[1], Wei XIAO[1], and Xuhui LEE[3]

[1]*Key Laboratory of Meteorological Disaster*, *Ministry of Education (KLME)/ Collaborative Innovation Center on Forecast and Evaluation of Meteorological Disasters (CIC-FEMD)/ Key Laboratory of Ecosystem Carbon Source and Sink*, *China Meteorological Administration (ECSS-CMA)/ Jiangsu Key Laboratory of Agricultural Meteorology*, *Nanjing University of Information Science & Technology*, *Nanjing* 210044, *China*

[2]*Key Laboratory of Urban Meteorology*, *China Meteorological Administration*, *Beijing* 100089, *China*

[3]*School of the Environment*, *Yale University*, *New Haven*, *CT* 06511, *USA*

ESM to: Lyu, H., W. Wang, K. Zhang, C. Cao, W. Xiao, and X. Lee, 2024: Factors influencing the spatial variability of air temperature urban heat island intensity in Chinese cities. *Adv. Atmos. Sci.*, **41**(5), 817−824, https://doi.org/10.1007/s00376-023-3012-y.

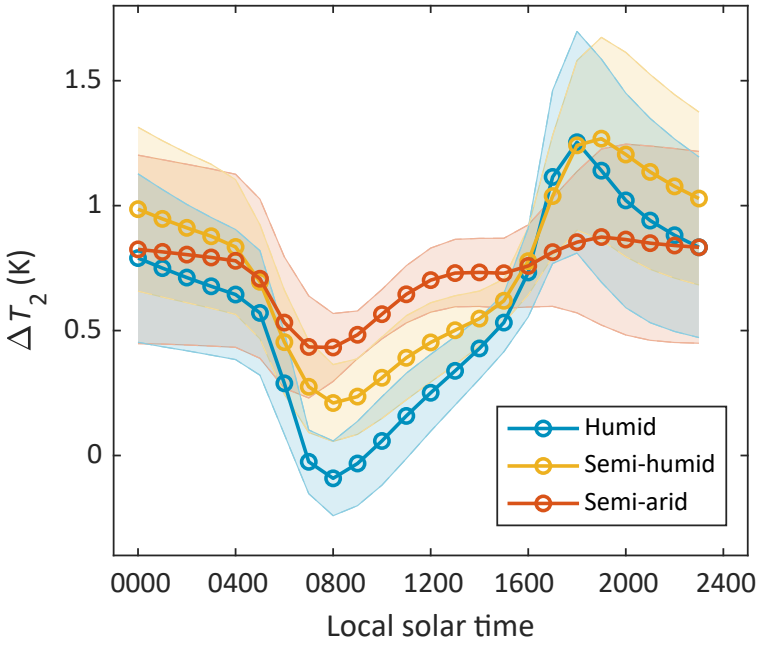

Fig. S1. Diurnal cycle of the AUHI for three climate zones across China. The shaded areas are one standard deviation of spatial variations.

*The online version of this article can be found at https://doi.org/10.1007/s00376-023-3012-y.

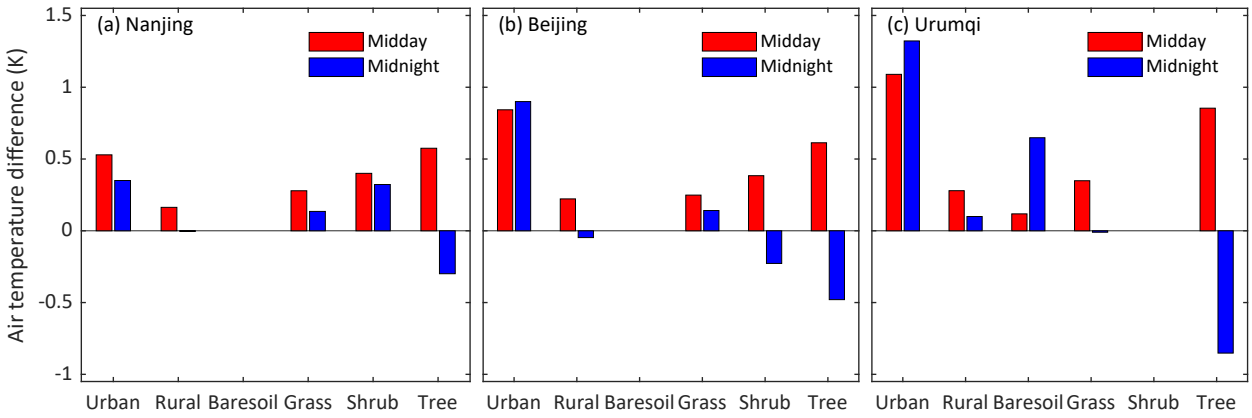

Fig. S2. Daytime and nighttime air temperature of subgrid tiles relative to the value of the crop tile in the same model grid. Three grids are shown, corresponding to Nanjing, Beijing and Urumqi. Reference air temperature of the crop tiles: Nanjing (daytime: 294.53 K; nighttime: 289.43 K); Beijing (daytime: 288.18 K; nighttime: 282.32 K); Urumqi (daytime: 285.61 K; nighttime: 279.57 K).

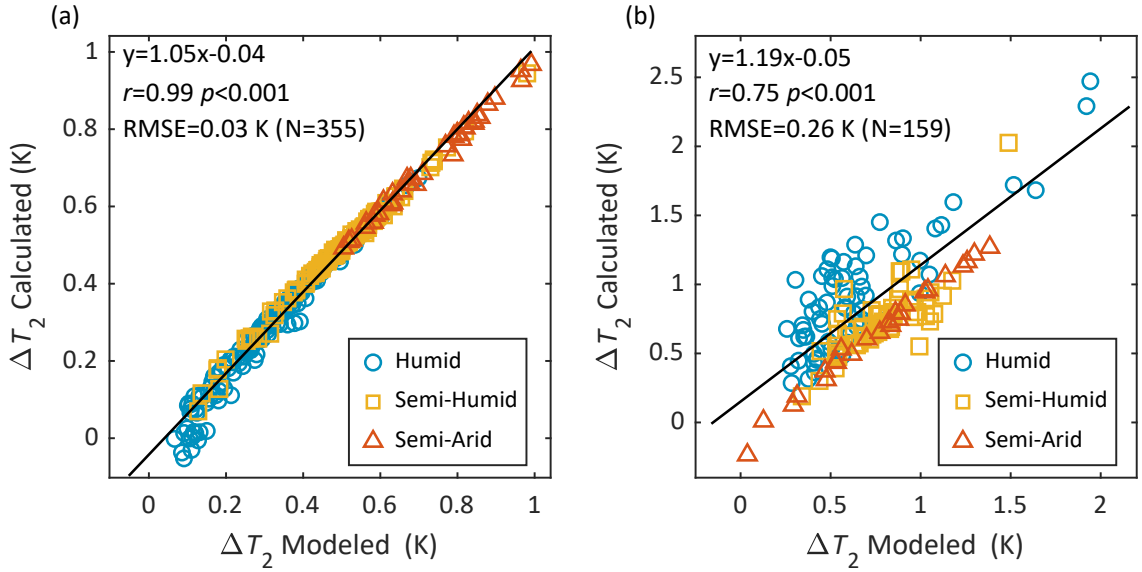

Fig. S3. Comparison between the modeled AUHI and offline AUHI calculated as the sum of component contributions for the (a) annual mean at midday and (b) annual mean at midnight. Each data point represents one pair of urban and rural tiles in the same grid cell.

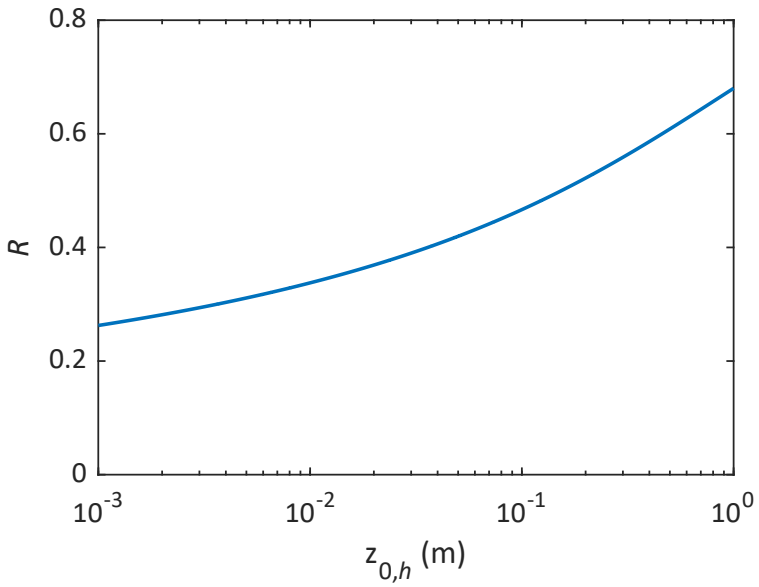

Fig. S4. Theoretical relationship between the resistance ratio R and thermal roughness $z_{0,h}$ in neutral stability.

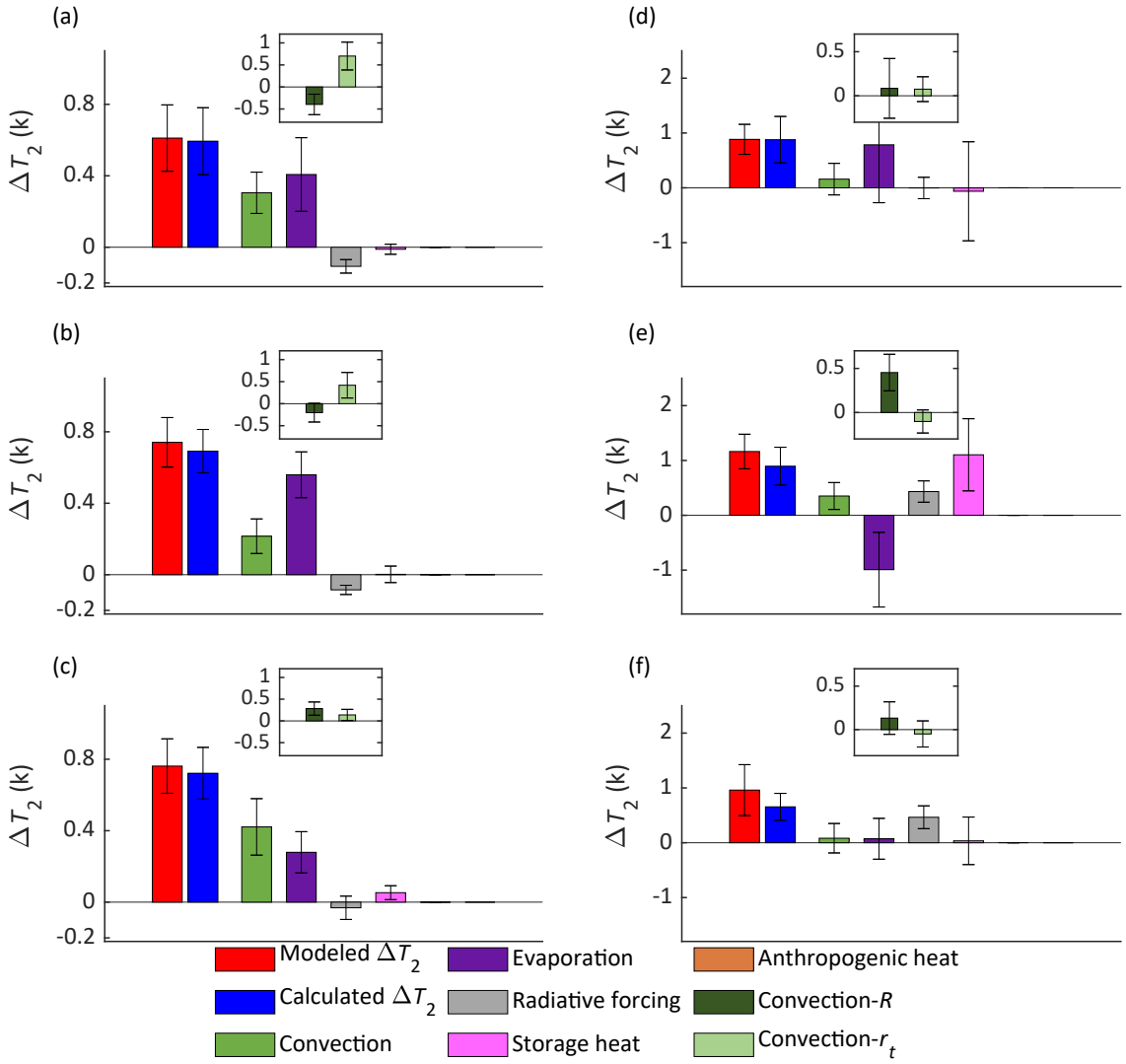

Fig. S5. Attribution of the summer AUHI in three climate zones. The summer-mean midday AUHI and its component contributions in the (a) humid, (b) semi-humid, and (c) semi-arid climate zone. The summer-mean midnight AUHI and its component contributions in the (a) humid, (b) semi-humid, and (c) semi-arid climate zone.

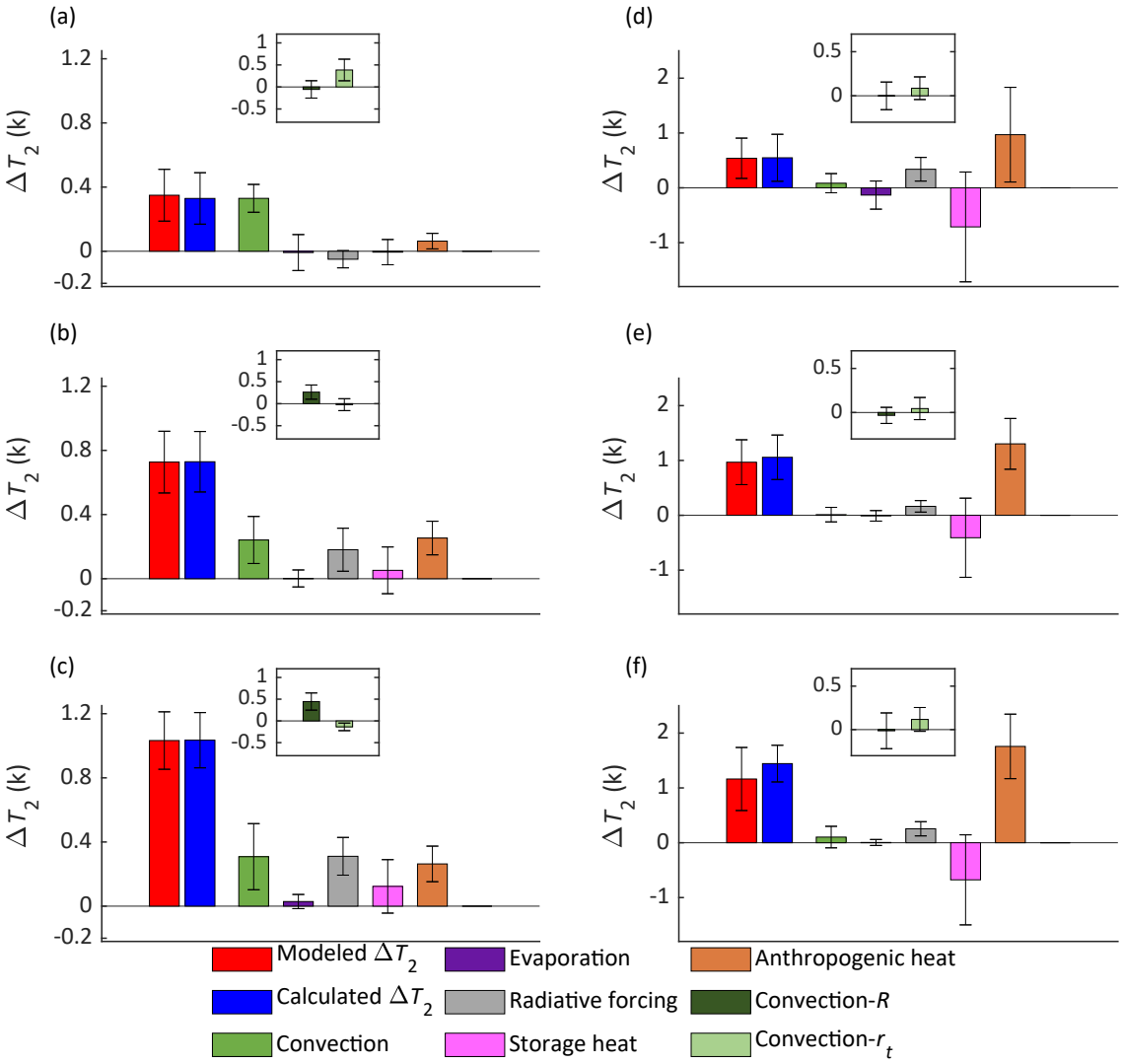

Fig. S6. Attribution of the winter AUHI in three climate zones. The winter-mean midday AUHI and its component contributions in the (a) humid, (b) semi-humid, and (c) semi-arid climate zone. The summer-mean midnight AUHI and its component contributions in the (a) humid, (b) semi-humid, and (c) semi-arid climate zone.

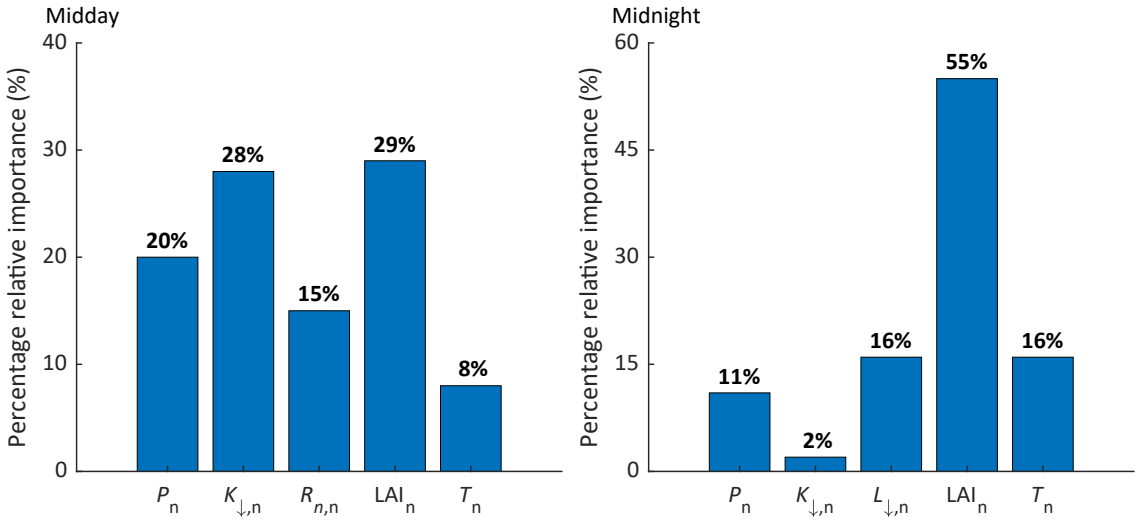

Fig. S7. Relative importance of predictors in explaining spatial variations in the midday and the midnight AUHI.

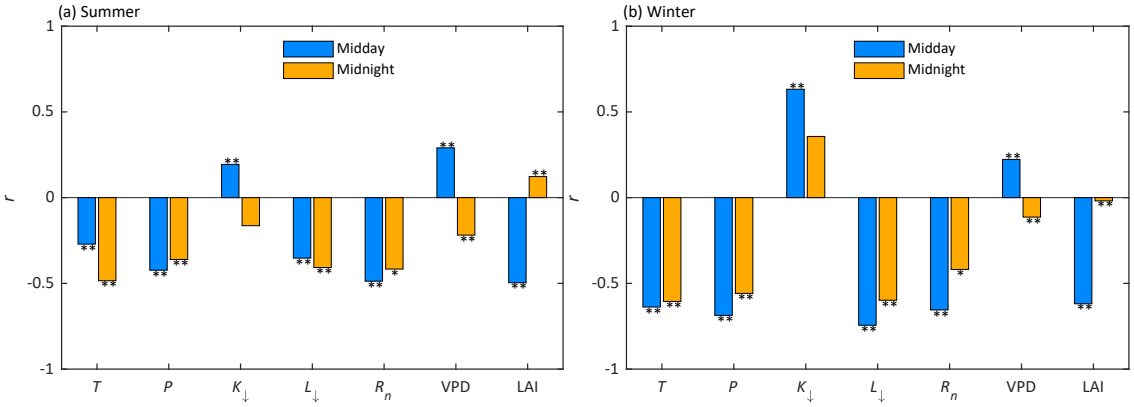

Fig. S8. Correlation coefficients between the summer (winter) mean midday and midnight AUHI and background drivers. T, annual mean temperature; P, annual mean precipitation; $K_{\downarrow}$, incoming solar radiation; $L_{\downarrow}$, incoming longwave radiation; R_n, net radiation; VPD, vapor pressure deficit; LAI, rural leaf area index. * and ** represent significance at the $p < 0.01$ and $p < 0.001$ confidence level, respectively.

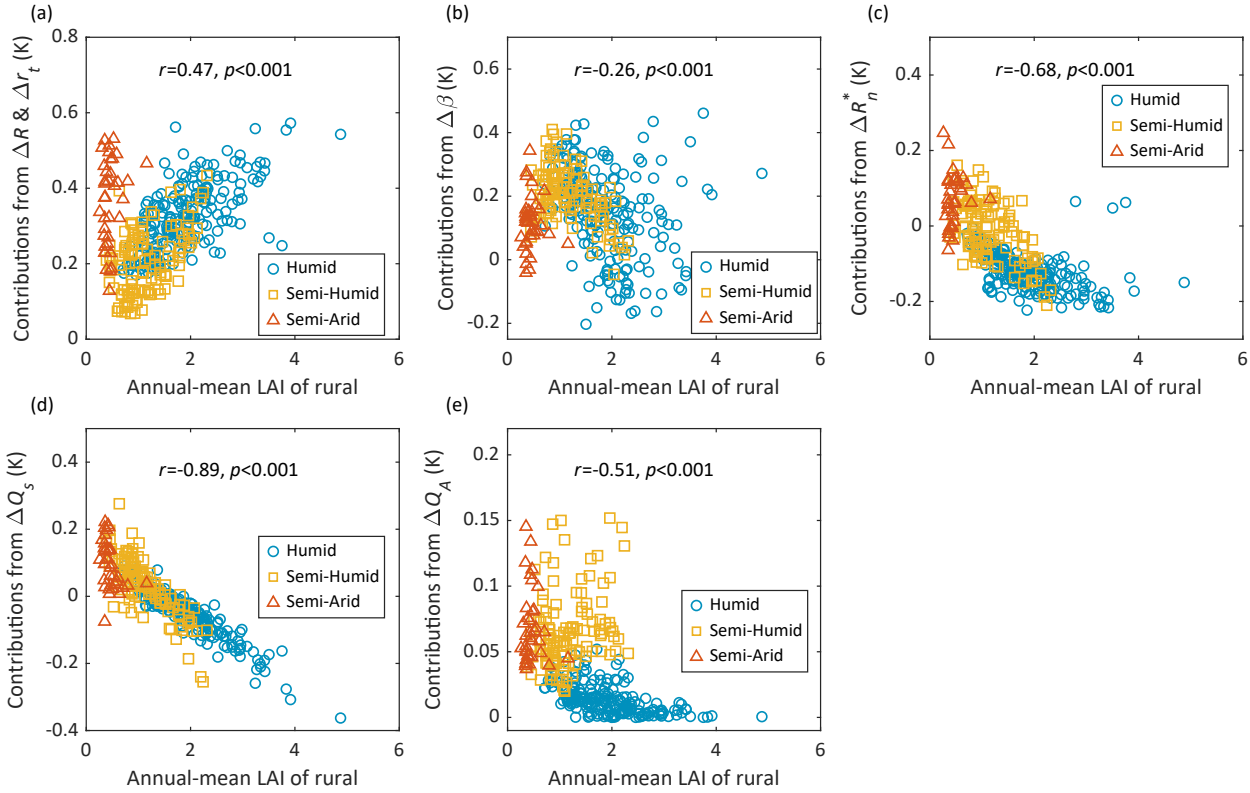

Fig. S9. Relationship of individual biophysical contributions to the midday AUHI with annual mean rural LAI. Each data point represents one pair of urban and rural tiles in a grid cell.

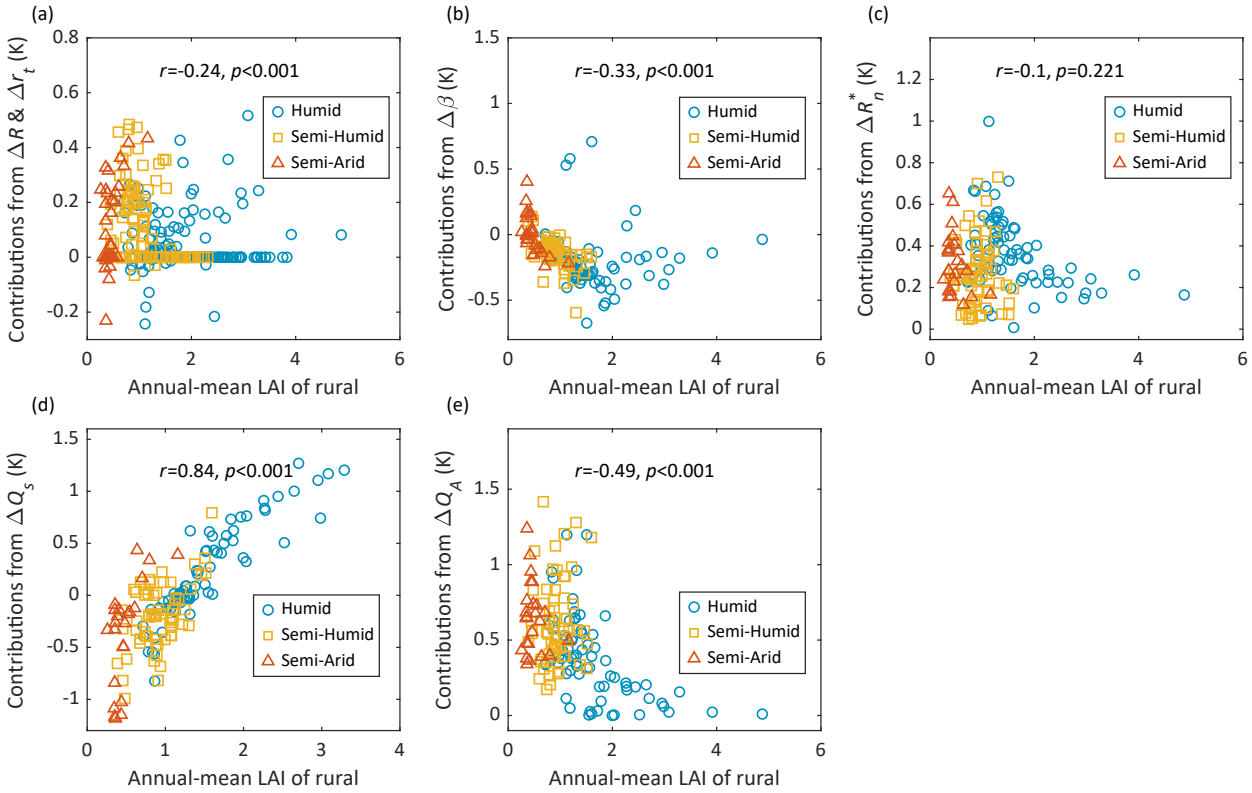

Fig. S10. Relationship of individual biophysical contributions to the midnight AUHI with annual mean rural LAI. Each data point represents one pair of urban and rural tiles in a grid cell.

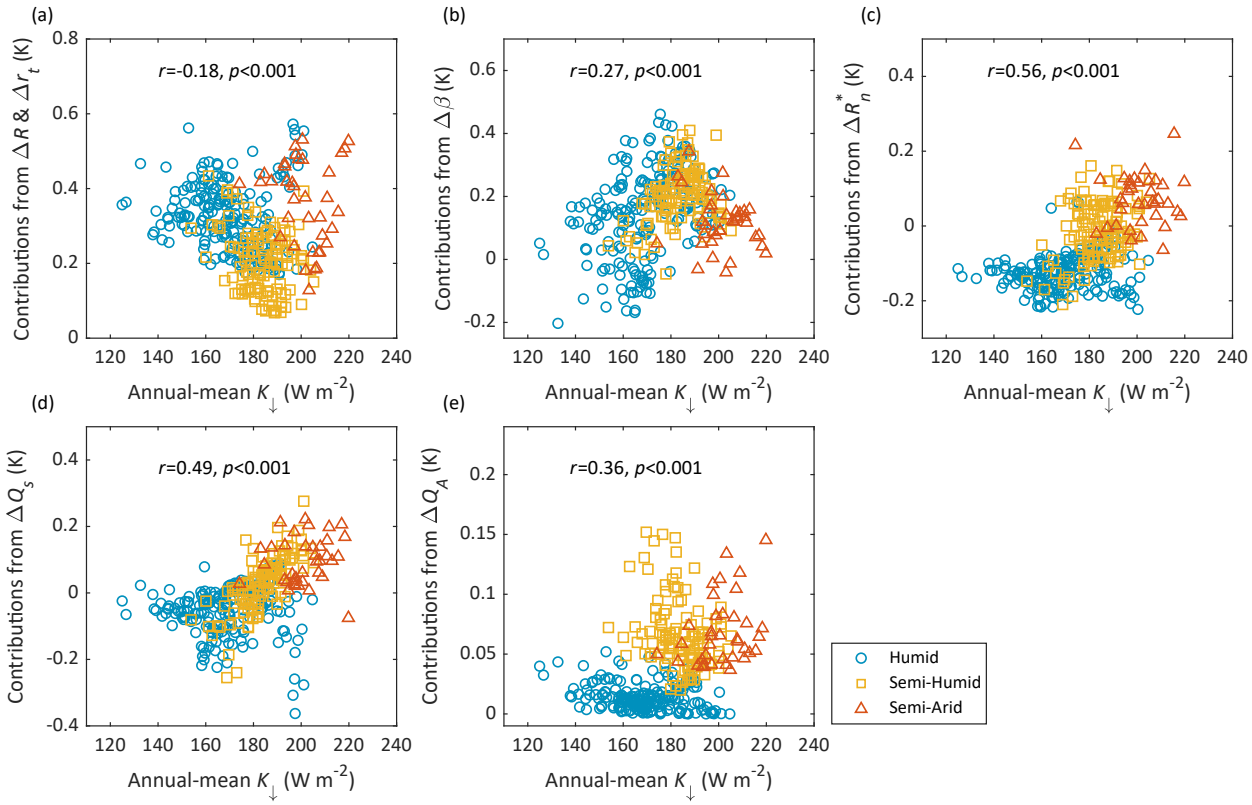

Fig. S11. Relationship of individual biophysical contributions to the midday AUHI with annual mean incoming solar radiation (units: W m^{-2}). Each data point represents one pair of urban and rural tiles in a grid cell.

Table S1. Summary of variables used in the attribution analysis. $K_{\downarrow}$, incoming solar radiation; $L_{\downarrow}$, incoming longwave radiation; R_n^*, apparent net radiation; T_b, air temperature at the blending height; f, energy redistribution factor; α, surface albedo; Q_s, storage heat flux; Q_A, anthropogenic heat flux; ε, surface emissivity; r_t, total resistance for heat transfer between the surface and the blending height; R, resistance ratio; β, Bowen ratio.

		Humid		Semi-humid		Semi-arid	
		urban	rural	urban	rural	urban	rural
Midday							
	$K_{\downarrow}$ (W m^{-2})	529.86		548.37		602.50	
	$L_{\downarrow}$ (W m^{-2})	372.58		295.23		291.12	
	R_n^* (W m^{-2})	401.41		376.34		405.49	
	T_b (K)	293.69		283.67		284.97	
	f	7.23		6.51		4.70	
	α	0.19	0.12	0.20	0.18	0.19	0.20
	Q_s (W m^{-2})	90.49	79.10	93.20	99.88	106.82	125.27
	Q_A (W m^{-2})	3.42	0	14.29	0	12.87	0
	ε	0.88	0.97	0.90	0.97	0.89	0.97
	r_t (s m^{-1})	69.66	37.47	60.65	46.63	57.4	54.14
	R	0.16	0.22	0.17	0.18	0.17	0.14
	β	1.20	0.91	2.40	1.42	4.17	2.93
Midnight							
	$K_{\downarrow}$ (W m^{-2})	—		—		—	
	$L_{\downarrow}$ (W m^{-2})	343.20		284.09		273.71	
	R_n^* (W m^{-2})	−50.14		−68.65		−78.65	
	T_b (K)	289.29		281.71		281.78	
	f	1.09		0.50		0.47	
	α	—	—	—	—	—	—
	Q_s (W m^{-2})	−46.97	−42.52	−55.08	−57.13	−59.99	−66.55
	Q_A (W m^{-2})	4.67	0	12.28	0	11.25	0
	ε	0.88	0.97	0.90	0.97	0.89	0.97
	r_t (s m^{-1})	89.42	141.70	90.51	154.33	99.57	218.79
	R	0.35	0.54	0.28	0.46	0.39	0.42
	β	−0.59	−1.68	−0.86	−1.88	−1.48	−1.84